Supplement of Atmos. Chem. Phys., 22, 2553–2568, 2022
https://doi.org/10.5194/acp-22-2553-2022-supplement

Supplement of

Urban inland wintertime N_2O_5 and $ClNO_2$ influenced by snow-covered ground, air turbulence, and precipitation

Kathryn D. Kulju et al.

Correspondence to: Kerri A. Pratt (prattka@umich.edu)

S1. Box model details

A simple box model was used to explore the impacts of aerosol surface area, temperature, pressure, and [O_3] on N_2O_5 and $ClNO_2$ mole ratios for the case study nights. In addition, the model was used to explore the relative importance of VOCs on NO_3 loss (Fig S14). This model does not consider the impacts of fog, rainfall, snowfall, ground cover, turbulence, or advection. Note that no clear correlation was observed between N_2O_5 and $ClNO_2$ mole ratios and wind speed or wind direction (Fig. S13). Simulations were conducted over 14 h to examine the 18:00-08:00 EST nighttime period for each case night.). Temperature, pressure, and aerosol surface area (14.1-736.5 nm) (*Sections 2.1 and 2.4*) were set to be constant and equal to the observed averages from 18:00-08:00 EST for each case night (Table S3). The model was initialized with 0 ppt for NO_3, HNO_3, $ClNO_2$, and N_2O_5, and an initial O_3 mole ratio equal to the observed average from 18:00-08:00 EST for each case night (*Section 2.2*, Table S3). The initial NO mole ratio was set to be 20 ppt, with 10 ppt h^{-1} added to account for emissions from the contributions of vehicles from the nearby roadway; these values were chosen so that the modeled concentrations of NO_2 and O_3 were relatively stable throughout the 14 h simulations. When discussing the results of the simulation with respect to mole ratios of N_2O_5 and $ClNO_2$ for the case study nights (Fig S15-16), we discuss the average of the last 4 h of each simulation (i.e. 04:00-08:00); this was done to give the model time to reach steady state, at which point the results are less dependent on the initial conditions.

Following the approach of Kenagy et al. (2020), the model considers the following reactions, with rate constants from the Master Chemical Mechanism, MCM v 3.3.1 (Saunders et al., 2003):

$$NO + O_3 \rightarrow NO_2 + O_2 \quad \text{(R-S1)}$$
$$NO + NO_3 \rightarrow 2\,NO_2 \quad \text{(R-S2)}$$
$$NO_2 + O_3 + M \rightarrow O_2 + NO_3 \quad \text{(R-S3)}$$
$$NO_3 + VOCs \rightarrow products \quad \text{(R-S4)}$$
$$NO_2 + NO_3 + M \rightleftharpoons N_2O_5 \quad \text{(R-S5)}$$
$$N_2O_5 + H_2O \rightarrow 2HNO_3 \quad \text{(R-S6)}$$
$$N_2O_5 + Cl^- \rightarrow ClNO_2 + NO_3^- \quad \text{(R-S7)}$$

We use the reaction rate constant k_{hyd} for hydrolysis of N_2O_5 during its heterogeneous reaction (R-S6 and R-S7) and define it as follows based on Bertram and Thornton (2009):

$$k_{hyd} = \frac{\bar{c} \times S_a \times \gamma}{4} \quad \text{(E-S1)}$$

$\bar{c}$ is the temperature-dependent mean molecular speed of N_2O_5, S_a is the measured aerosol surface area concentration, and γ is the reactive uptake coefficient for N_2O_5.

To estimate the VOC reactivity to NO_3, we refer to previous measurements of light hydrocarbons (C_2H_6, C_3H_8, n-C_4H_{10}, i-C_4H_{10}, HCHO, and CH_3CHO) in Ann Arbor, MI during Feb. 2016 (McNamara et al., 2020). Considering the NO_3 rate constants reported by the National Institute of Standards and Technology kinetics database, we estimate the VOC reactivity to NO_3 to be 3.6×10^{-4} s^{-1}. Therefore, for the SNACK study the VOC reactivity to NO_3 was likely between 1×10^{-4} s^{-1} and 1×10^{-3} s^{-1}.

Since NO_2 was not measured in Kalamazoo, MI during the SNACK study, we refer to the previously simulated [NO_2] by Wang et al. (2020) using measured [NO] and [O_3] during February 2016 in Ann Arbor, MI. This previous study simulated a median nighttime [NO_2] of 31 ppb, with the 25th and 75th percentiles equal to 9.4 ppb and 59 ppb, respectively. Therefore, in the current study, we explore a [NO_2] range of 100 ppt – 100 ppb in our modeling (Fig S14-S16). We intentionally explore a larger range of VOC reactivity and [NO_2] than we expect was observed in wintertime MI, such that 1) the true conditions at the sampling site were likely captured and 2) the impacts of extreme conditions (e.g. very low VOC reactivity+very low [NO_2], very high VOC reactivity+very high [NO_2], etc.) are still shown such that the reader can see how those extreme conditions would influence our box model results.

The box model also includes N_2O_5 uptake (γ) and $ClNO_2$ yield (φ) onto aerosol particles (Bertram and Thornton, 2009). The average γ reported from Ann Arbor, MI in Feb – Mar 2016 was 0.0155, and the average φ was 0.24 ($\gamma\times\varphi$ product = 0.0037) (McNamara et al., 2020). Therefore, for the modeling herein, we explore a $\gamma\times\varphi$ product range of 0.0001 (10^{-4}, e.g. γ=0.001 and φ=0.1) – 0.01 (10^{-2}, e.g. γ=0.01 and φ=1) (Fig S14).

S2. Discussion of Box Model Results

As shown in Fig. S14, when [NO_2] = 31 ppb (median during Feb. 2016 in Ann Arbor, MI (McNamara et al., 2020)), >95% of NO_3 is simulated to be lost through the inorganic pathways (production of HNO_3 and $ClNO_2$, compared to reaction with VOCs) for all VOC reactivities to NO_3 up to 10^{-3} s^{-1} and across all case studies (Fig S14). In fact, for all cases but one (rainfall), >95% of NO_3 is also lost through the inorganic pathways for VOC reactivities up to 10^{-3} s^{-1} at [NO_2] = 9.4 ppb, which corresponds to the 25th percentile from another study in February 2016 in Ann Arbor, MI (McNamara et al., 2020). For the one exception (rainfall case), the 95th percentile for NO_3 lost through the inorganic pathways occurs at [NO_2] = 16 ppb and at a VOC reactivity to NO_3 of 10^{-3} s^{-1}, with the 90th percentile occurring at [NO_2] = 4.5 ppb. Therefore, we conclude that the VOC loss pathway for NO_3 is likely minor in this wintertime urban MI environment.

Since the model does not include fog, rainfall, or snowfall, we expect that the clear case study night should be best represented by the model. At NO_2 and $\gamma*\varphi$ levels corresponding to Feb. 2016 in Ann Arbor, MI (NO_2=31 ppb and $\gamma*\varphi$=0.0037) (McNamara et al., 2020), the simulated N_2O_5 mole ratio is 150 ppt (Fig. 6). In comparison, the minimum, average, and maximum N_2O_5 mole ratios observed from 04:00-08:00 EST on the clear case study night were 191 ppt, 229 ppt, and 274 ppt, respectively. As shown in Fig. S15, the mean observations of N_2O_5 from 04:00-08:00 EST were simulated by the model to occur at NO_2=9.1 ppb and $\gamma*\varphi=10^{-2}$ (e.g. γ=0.01 and φ=1), and NO_2=1.9 ppb and $\gamma*\varphi=10^{-4}$ (e.g. γ=0.001 and φ=0.1), which are plausible. However, the box model may be missing an N_2O_5 source due to the possible underprediction of N_2O_5 mole ratios during the clear case.

For the fog case study model results, the observed minimum, average, and maximum N_2O_5 mole ratios from 04:00-08:00 EST (1.2 ppt, 1.9 ppt, and 2.7 ppt, respectively,, Fig. 6) were not simulated to occur within reasonable model inputs (i.e. off-scale in Fig. S15). Considering the median [NO_2] = 31 ppb and a $\gamma*\varphi$ product of 0.0037 during Feb. 2016 in Ann Arbor, MI (McNamara et al., 2020), the model predicts 135 ppt of N_2O_5. Yet, even at 100 ppt of NO_2 (unrealistically low) and $\gamma*\varphi=10^{-2}$ (e.g. γ=0.01 and φ=1), 3.4 ppt of N_2O_5 is simulated. This shows that the wide range of possible model conditions still overpredicts N_2O_5 abundance. Since NO_2 was likely >100 ppt in abundance, γ was likely <0.01, and φ

was likely <1 (*Sect. S1*), this supports fog droplet scavenging as a missing N_2O_5 sink (i.e. scavenging) earlier in the night. Yet, the maximum observed N_2O_5 mole ratio from 04:00 – 08:00 EST of the fog case night was 2.7 ppt (Fig. 6).

For the rainfall case study, the wide range of possible model conditions still overpredicts N_2O_5 abundance, similar to the fog case night. At a $\gamma*\varphi$ product of 0.0037 (McNamara et al., 2020), an unrealistically low NO_2 mole ratio (~100 ppt) would be required (Fig. S15) to reach the average N_2O_5 mole ratio of 9.5 ppt observed between 04:00 and 08:00 EST on the rainfall case night (Fig. 6). Since NO_2 was likely >100 ppt in abundance, a missing sink (scavenging/wet deposition) of N_2O_5 is likely during the rainfall case. Considering the median $[NO_2]$ = 31 ppb and a $\gamma*\varphi$ product of 0.0037 from our previous wintertime Ann Arbor, MI study (McNamara et al., 2020) results in 380 ppt of N_2O_5 simulated (Fig. 6). Yet, the maximum observed N_2O_5 mole ratio from 04:00 – 08:00 EST of the rainfall case night was 11.4 ppt (Fig. 6).

N_2O_5 abundance during the snowfall case was also overpredicted by the model, again implying a missing sink (scavenging/wet deposition). At a $\gamma*\varphi$ product of 0.0037 (*Sect. S1*), an unrealistically low NO_2 mole ratio (~630 ppt) would be required (Fig. S15) to reach the average observation of N_2O_5 from the last 4 h of the snowfall case. Applying the median $[NO_2]$ = 31 ppb and a $\gamma*\varphi$ product of 0.0037 from the previous wintertime Ann Arbor, MI study (McNamara et al., 2020) leads to 190 ppt of N_2O_5 based on these simulations. However, the maximum observed from 04:00-08:00 EST of the snowfall case was 34.2 ppt.

For the clear case study model results shown in Fig. S16, the mean $ClNO_2$ mole ratio from 04:00-08:00 EST (39.0 ppt) was simulated for NO_2=270 ppt and $\gamma*\varphi=10^{-2}$ (e.g. γ=0.01 and φ=1) and NO_2=9.1 ppb and $\gamma*\varphi=10^{-4}$ (e.g. γ=0.001 and φ=0.1), the latter of which corresponds to realistic values. At NO_2 and $\gamma*\varphi$ levels corresponding to Feb. 2016 in Ann Arbor, MI (NO_2=31 ppb and $\gamma*\varphi$=0.0037) (McNamara et al., 2020), the simulated $ClNO_2$ mole ratio was 280 ppt. However, the minimum, average, and maximum $ClNO_2$ mole ratios observed from 04:00-08:00 EST were 35.8 ppt, 39.0 ppt, and 45.2 ppt, respectively (Fig. 6). Notably, the box model overpredicted $ClNO_2$ mole ratios during the clear case for the prior Ann Arbor conditions, despite having underpredicted N_2O_5 mole ratios under the same conditions. This points to the variability and need to better constrain $\gamma*\varphi$ (N_2O_5 uptake and $ClNO_2$ yield).

The maximum observed $ClNO_2$ mole ratio from the last 4 h of the fog case study (04:00 – 08:00 EST) was 2.5 ppt. Applying the median $[NO_2]$ = 31 ppb and a $\gamma*\varphi$ product of 0.0037 from Ann Arbor, MI during Feb. 2016 (McNamara et al., 2020) results in 140 ppt of $ClNO_2$ being simulated (Fig. 6). At a $\gamma*\varphi$ product of 0.0037, an unrealistically low value of 100 ppt of NO_2 would still produce 7.3 ppt of $ClNO_2$ (Fig. S16). A $\gamma*\varphi$ product of $<10^{-3}$ (0.001) and $[NO_2]$ = 100 ppt would be required to match the average observation of $ClNO_2$ (2.1 ppt) from 04:00 – 08:00 EST. However, NO_2 was likely >100 ppt in abundance, and the $\gamma*\varphi$ product was likely $\geq 10^{-3}$. This overprediction of $ClNO_2$ mole ratios, by ~50 times, was similar to the overprediction of N_2O_5 mole ratios, further supporting fog droplet N_2O_5 scavenging, not represented by the model, as the reason for the $ClNO_2$ overprediction.

The maximum observed $ClNO_2$ mole ratio from the last 4 h of the rainfall case study (04:00 – 08:00 EST) was 3.2 ppt. Applying the median $[NO_2]$ = 31 ppb and a $\gamma*\varphi$ product of 0.0037 from Ann Arbor, MI during Feb. 2016 (McNamara et al., 2020) results in the simulation of 280 ppt of $ClNO_2$ (Fig. 6). At a $\gamma*\varphi$ product of 0.0037, an unrealistically low value of 100 ppt of NO_2 would still produce 5.0 ppt of $ClNO_2$(Fig. S16). Since NO_2 was likely >100 ppt in abundance, this suggests a missing sink (scavenging) for the rainfall case, similar to the fog droplet case. This overprediction of $ClNO_2$ mole ratios (by ~90 times) was larger than the overprediction of N_2O_5 mole ratios (by ~30 times) during the rainfall case, suggesting that $ClNO_2$, in addition to N_2O_5, is scavenged by the rain droplets.

For the snowfall case, applying the median $[NO_2]$ = 31 ppb and a $\gamma*\varphi$ product of 0.0037 from Ann Arbor, MI during Feb. 2016 (McNamara et al., 2020) results in 400 ppt of $ClNO_2$ being simulated. However, the maximum observed $ClNO_2$ mole ratio during the final 4 h of the snowfall case (04:00 – 08:00 EST) was 33.6 ppt. The box model overpredicted $ClNO_2$ mole ratios during the snowfall case (by ~12 times, as compared to ~5 times for N_2O_5 mole ratios). At a $\gamma*\varphi$ product of 0.0037 (*Sect. S1*), a low mole ratio of ~200 ppt of NO_2 would be required to reach the average observation of $ClNO_2$ from the last 4 h of the snowfall case (27.2 ppt), suggesting a missing sink (scavenging) affecting both N_2O_5 and $ClNO_2$ abundance during the snowfall case.

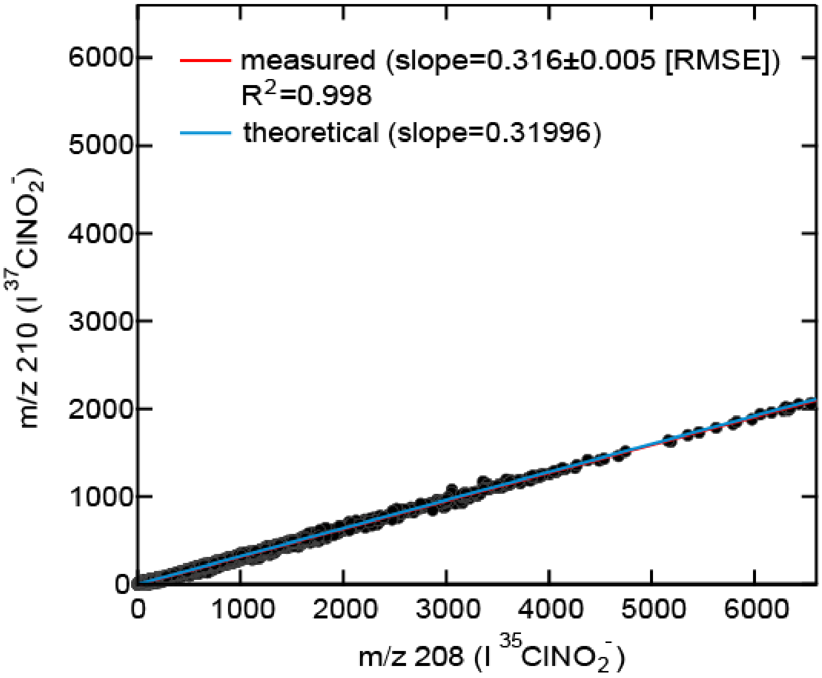

Figure S1: Plot of 5-min averaged, background subtracted, signals for m/z 210 vs. m/z 208, showing the isotopic ratio used to identify $ClNO_2$.

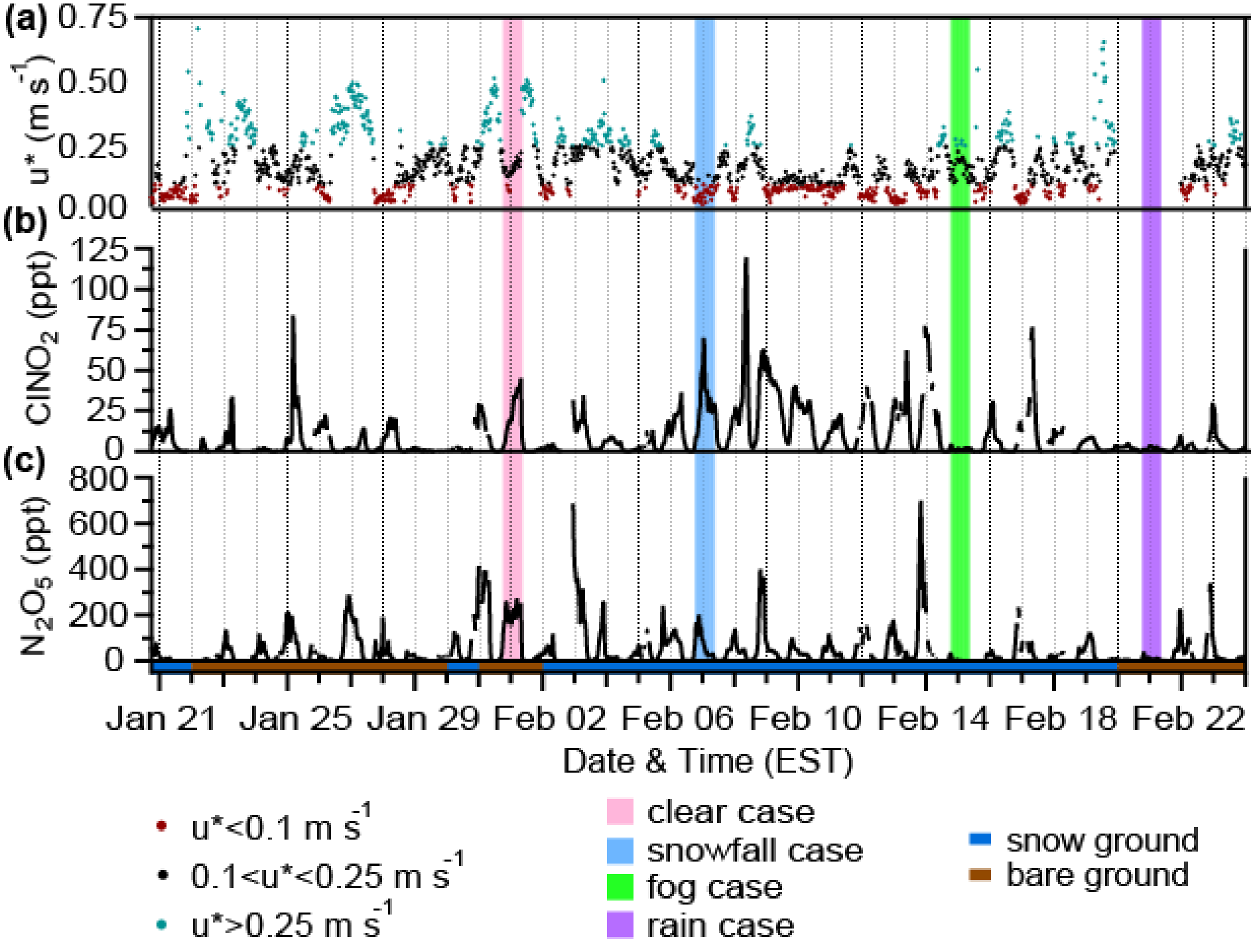

Figure S2: 30 min averaged (a) friction velocities (u*, m s^{-1}) and (b) $ClNO_2$ and (c) N_2O_5 mole ratios from January 20 to February 24, 2018. Friction velocities are divided into three categories: lower ($u^*<0.1$ m s^{-1}, red), intermediate ($0.1<u^*<0.25$ m s^{-1}, black), and higher ($u^*>0.25$ m s^{-1}, aqua). The shading below the x-axis represents ground cover – snow (blue) or bare ground (brown). Vertical shading represents the example case studies: clear (pink), snowfall (light blue), fog (green), and rain (purple). Gaps in the $ClNO_2$ and N_2O_5 timeseries are due to experiments described by (McNamara et al., 2021).

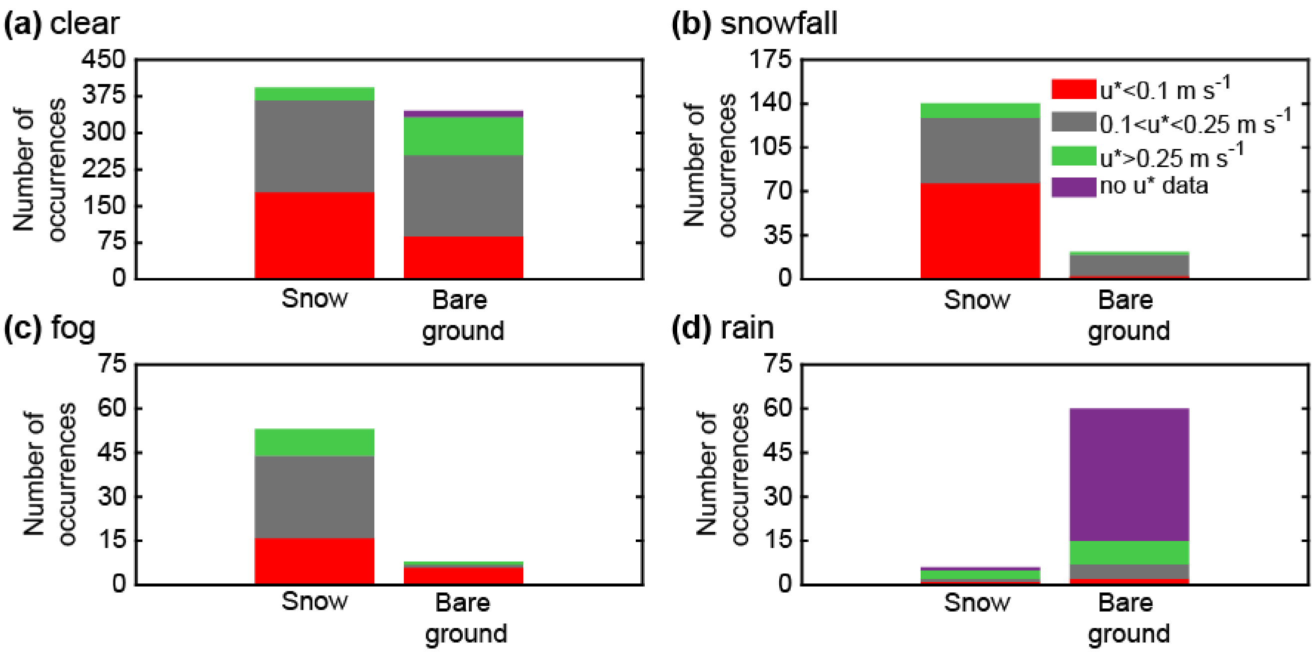

Figure S3: Stacked bar graphs showing the number of occurrences between 18:00 and 08:00 (30 min time resolution) of lower- ($u^{*}<0.1$ m s^{-1}), mid- ($0.1<u^{*}<0.25$ m s^{-1}), and higher-turbulence ($u^{*}>0.25$ m s^{-1}) over snow-covered and bare ground, during (a) clear, (b) snowfall, (c) fog, and (d) rainfall conditions. Lower turbulence occurred 39% of the time, mid-turbulence occurred 42% of the time, and higher turbulence occurred 14% of the time. Snowfall and fog both primarily occurred over snow-covered ground (87% of the time). Rainfall occurred over bare ground 92% of the time. Clear conditions had snow-covered and bare ground 58% and 42% of the time, respectively. Lower-turbulence accompanied snow-covered ground 71% of the time, and higher-turbulence accompanied bare ground 64% of the time. The most frequent turbulence bin to occur during snowfall and fog was $u_{*}<0.1$ m s^{-1}, representing 59% and 55% of the occurrences during these periods, respectively. Clear conditions had $0.1<u_{*}<0.25$ m s^{-1} as the most frequent bin, followed by $u_{*}<0.1$ m s^{-1}, representing 48% and 36% of these periods, respectively. In contrast, the most frequent turbulence bin to occur during rainfall was $u_{*}>0.25$ m s^{-1}, representing 17% of all occurrences during rain and 55% of the periods for which measurements were available. Sonic anemometer measurements, and therefore calculated u_{*} values, are unavailable from February 20-21.

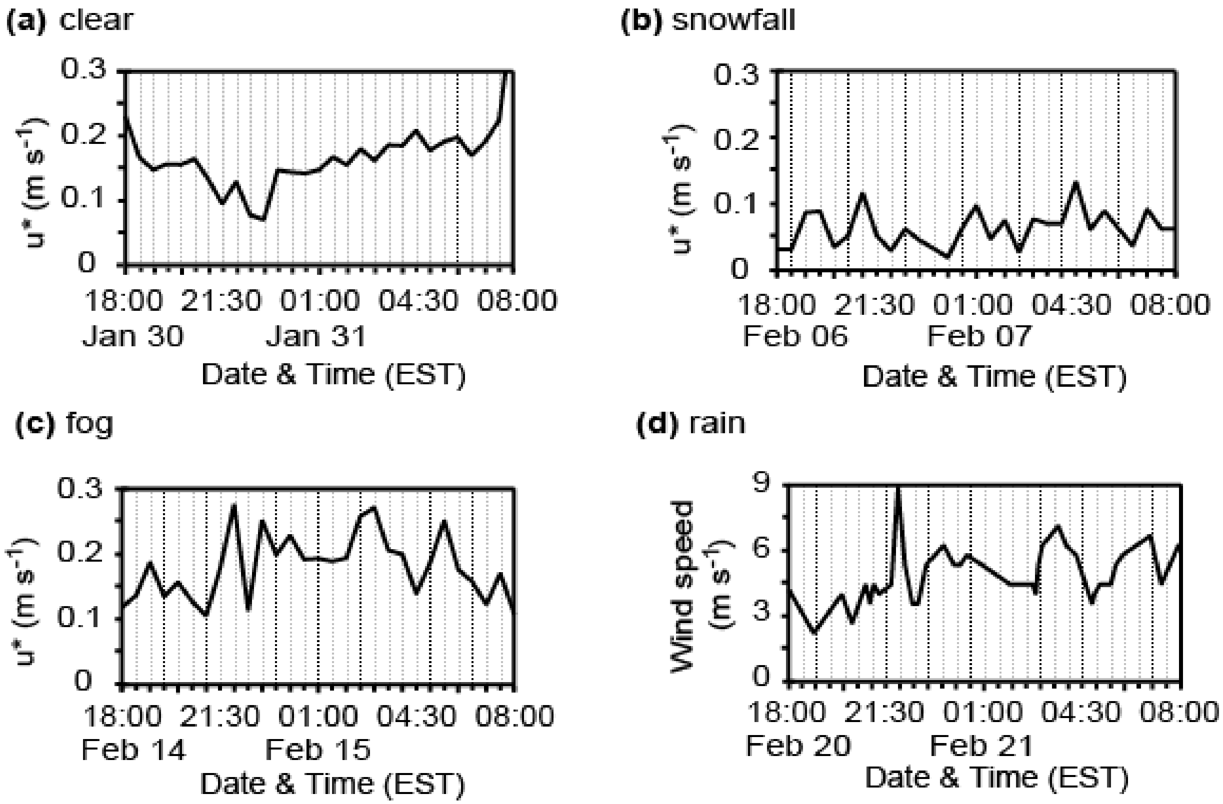

Figure S4: Friction velocity or wind speed between 18:00 and 08:00 h EST for each of the case studies presented – (a) clear, (b) snowfall, (c) fog, and (d) rainfall. Friction velocity could not be calculated for the rainfall case because sonic anemometer data were unavailable. Wind speed is substituted, and the relationship between wind speed and friction velocity is described in Figure S5.

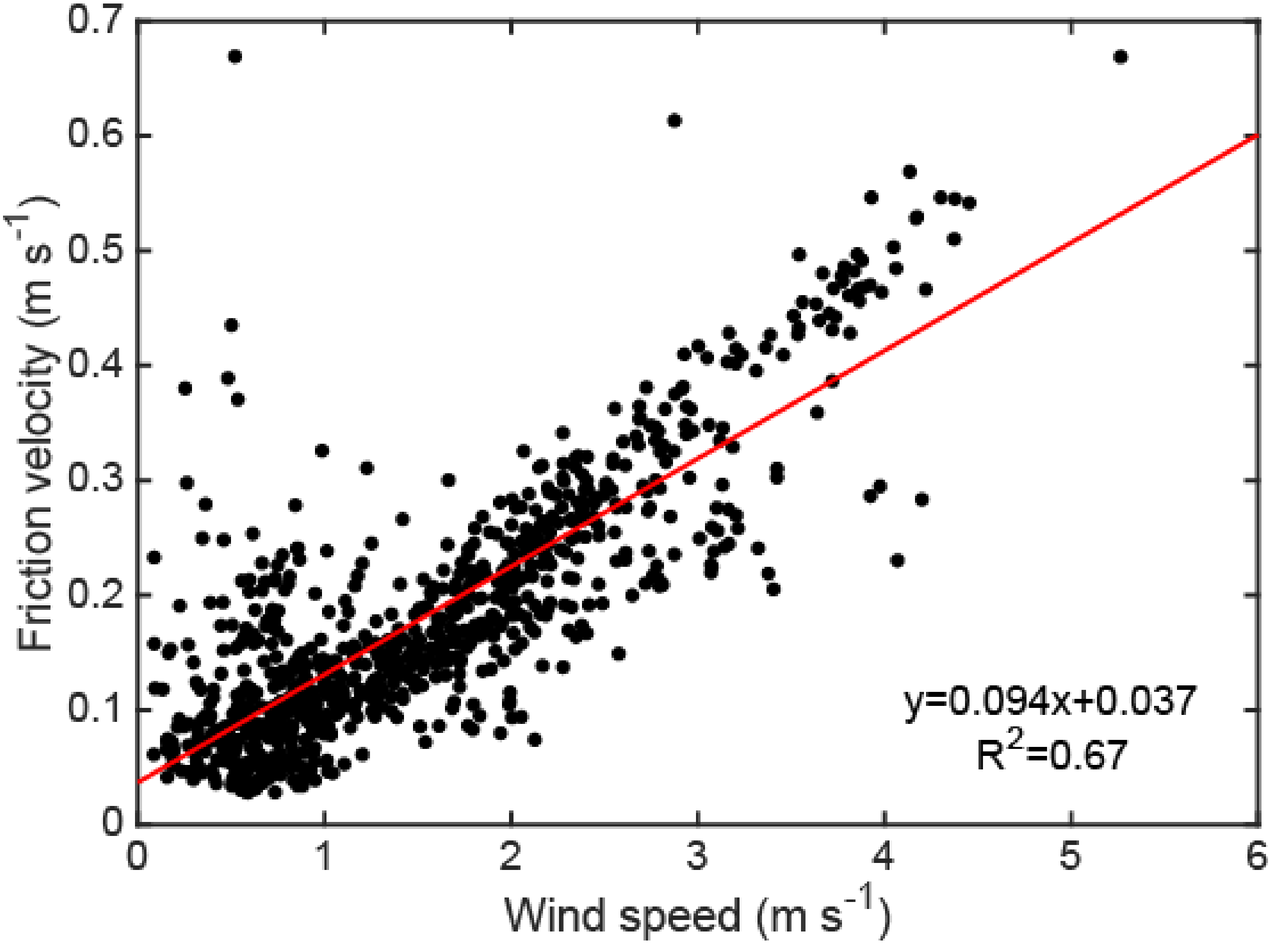

200 **Figure S5:** Relationship between friction velocity and wind speed, measured by the sonic anemometer at 20 Hz and plotted as 30-min averages. This linear regression indicates that for wind speed values greater than 2.3 m s^{-1}, the friction velocity was above 0.25 m s^{-1} (consistent with higher turbulence in the context of this study).

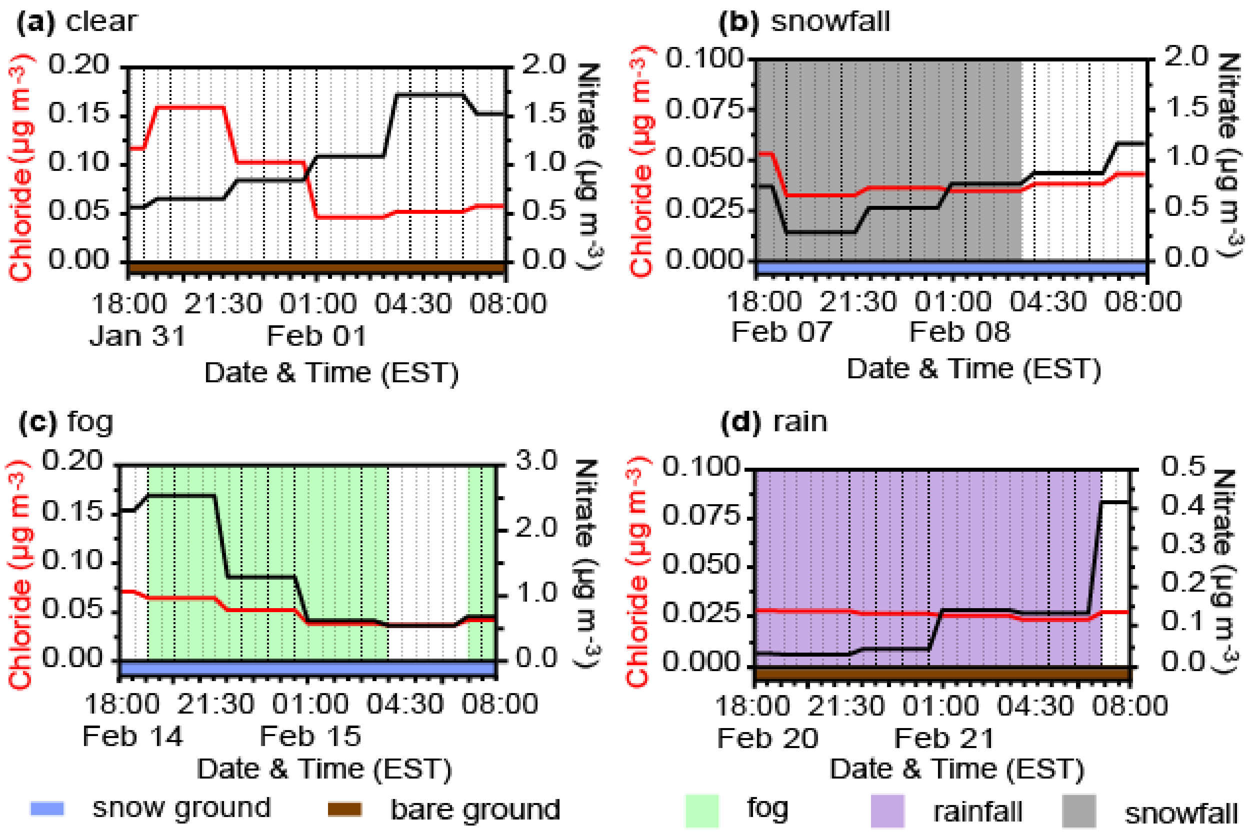

Figure S6: $PM_{2.5}$ chloride and nitrate concentrations between 18:00 and 08:00 h EST for each of the case studies presented – (a) clear air, (b) snowfall, (c) fog, and (d) rainfall. AIM-IC data were unavailable for the snowfall case night of February 06-07; therefore, we instead show a similar night, February 07-08 (the night after the snowfall case study) for comparison. The snowfall case study night and its substitution were similar in respect to snowfall and ground cover, but the substituted night had a higher friction velocity (average $u^* = 0.12$ m s^{-1}, whereas the snowfall case had an average $u^* = 0.06$ m s^{-1}).

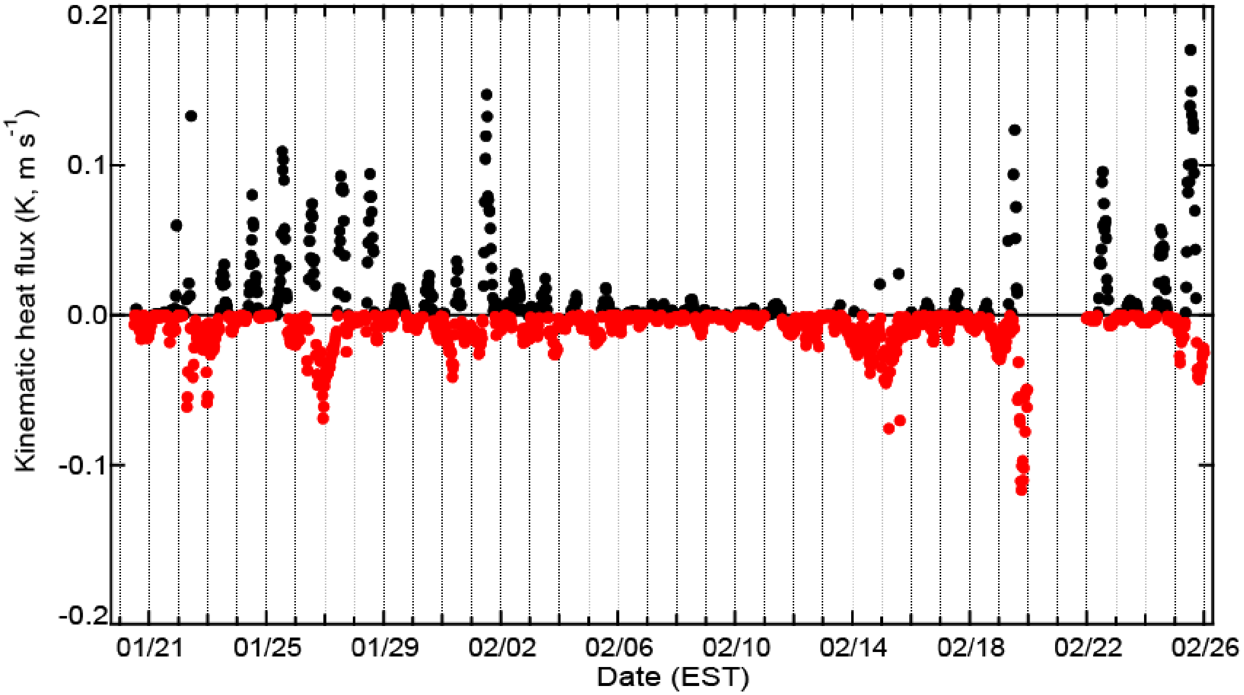

Figure S7: Temporal variation of 30 min averaged kinematic heat flux throughout the duration of the 215 study. Values less than zero, indicating a temperature inversion, are shown in red. A temperature inversion occurred during every night for which sonic anemometer data was available. Data sets were unavailable from 20 to 21 February due to complications associated with heavy rainfall.

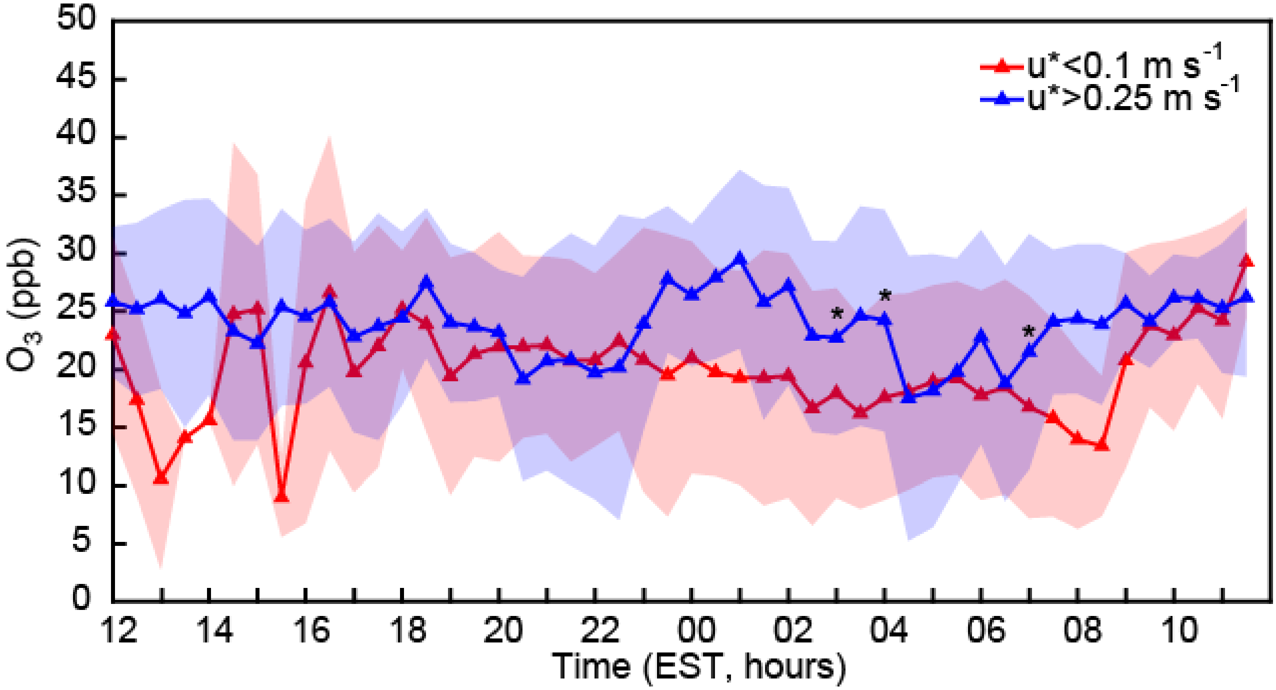

Figure S8: Diel patterns of 30 min averaged mole ratios of ozone (O_3) binned by lower ($u^* < 0.1$ m s^{-1}) and higher ($u^* > 0.25$ m s^{-1}) turbulence conditions from January 20 - February 24. Shading represents one standard deviation. Asterisks represent statistically significant (t-test) differences at the $p<0.05$ level between lower and higher turbulence conditions for each 30 min time period. Considering the statistically
225 significantly different periods of 03:00, 04:30, and 07:00 h, ozone mole ratios are 7.0 ppb (1.4-fold) higher during higher-turbulence, conditions, on average. For the entire nighttime period (18:00-08:00 h), much of which is not statistically significantly different between the two turbulence bins, ozone mole ratios were 3.2 ppb (1.2-fold) higher during higher-turbulence conditions, on average.

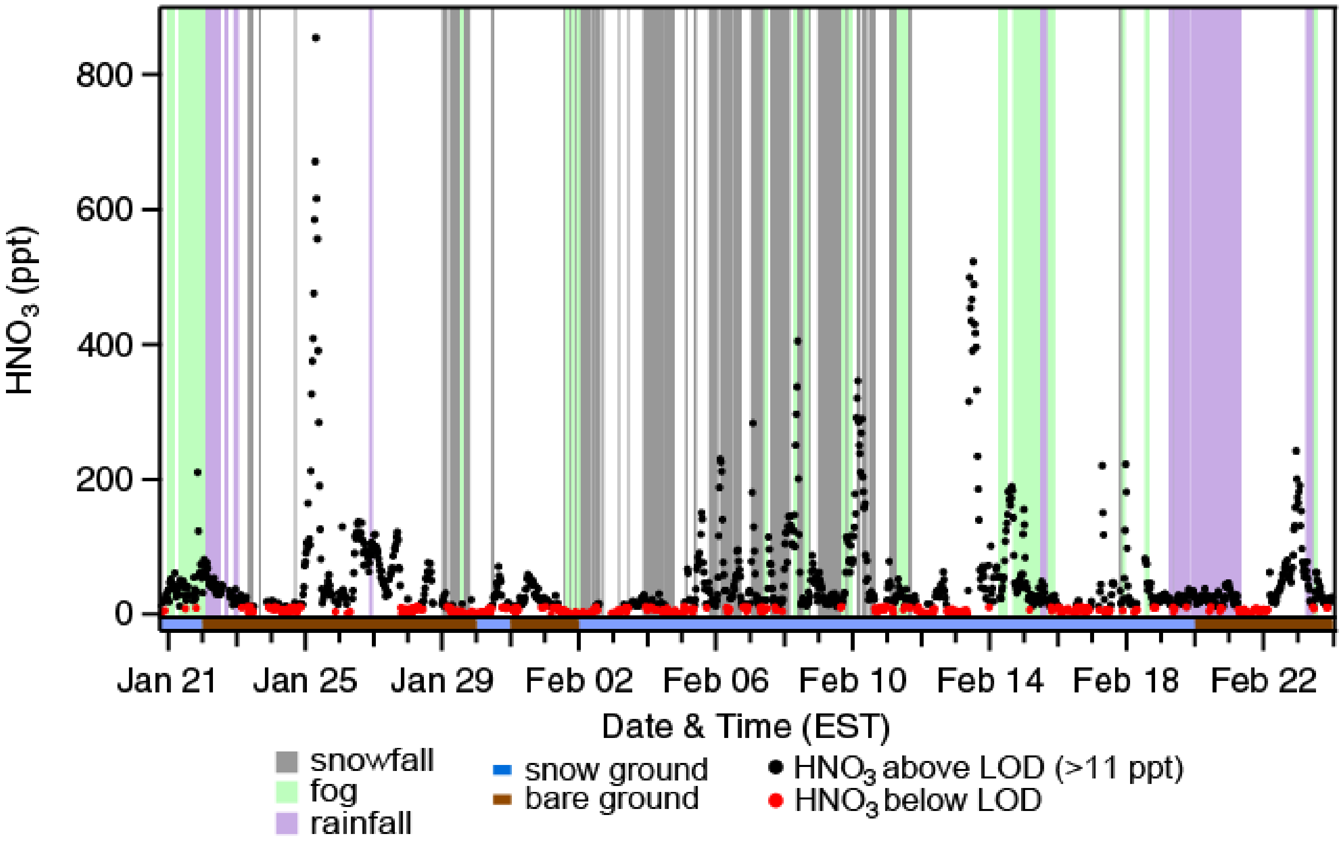

Figure S9: Mole ratios of 30 min averaged HNO3 during the campaign, and occurrence of snowfall (gray), fog (green), and rainfall (purple). The shading below the x-axis represents ground cover – snow (blue) or bare ground (brown). Considering periods between 18:00 and 08:00 EST when HNO3 was above LOD, where n=number of 30 min periods, the air was clear 63% of the time [n=376], snowfall occurred 18% of the time [n=105], rainfall occurred 10% of the time [n=60], and fog occurred 9% of the time [n=52]. The total number of 30 min periods for which HNO3 was above LOD during nighttime was 593, or 60% of the nighttime data during the campaign. These data represent lower limits as they were not adjusted for the poor background scrubbing efficiency of 12±1%, and therefore, should only be viewed qualitatively.

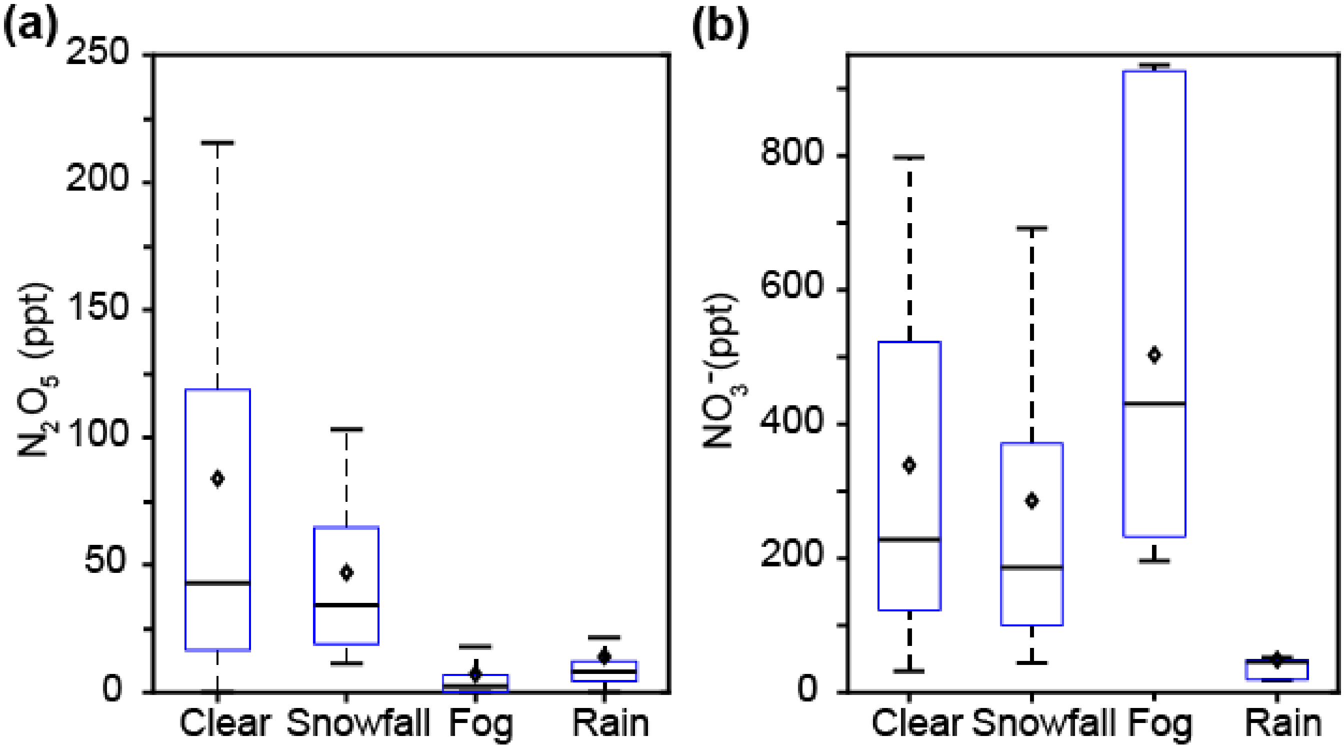

Figure S10: Box plots showing 30 min averaged mole ratios of (a) N_2O_5 and (b) $PM_{2.5}$ NO_3^- during clear conditions and weather events (snowfall, fog, and rain) from January 20-February 24. Bars represent the 10th, 50th, and 90th percentiles, boxes represent the 25th and 75th percentiles, and diamonds represent the means. Only nighttime data between 18:00 and 08:00 h EST are included. The purpose of this figure is to show how the decrease in N_2O_5 compares to the increase in NO_3^- during fog in units that are appropriate for direct comparison. During fog, N_2O_5 mole ratios were lower by 77±5 ppt, and $PM_{2.5}$ NO_3^- mole ratios were higher by 160±20 ppt, in comparison to clear conditions.

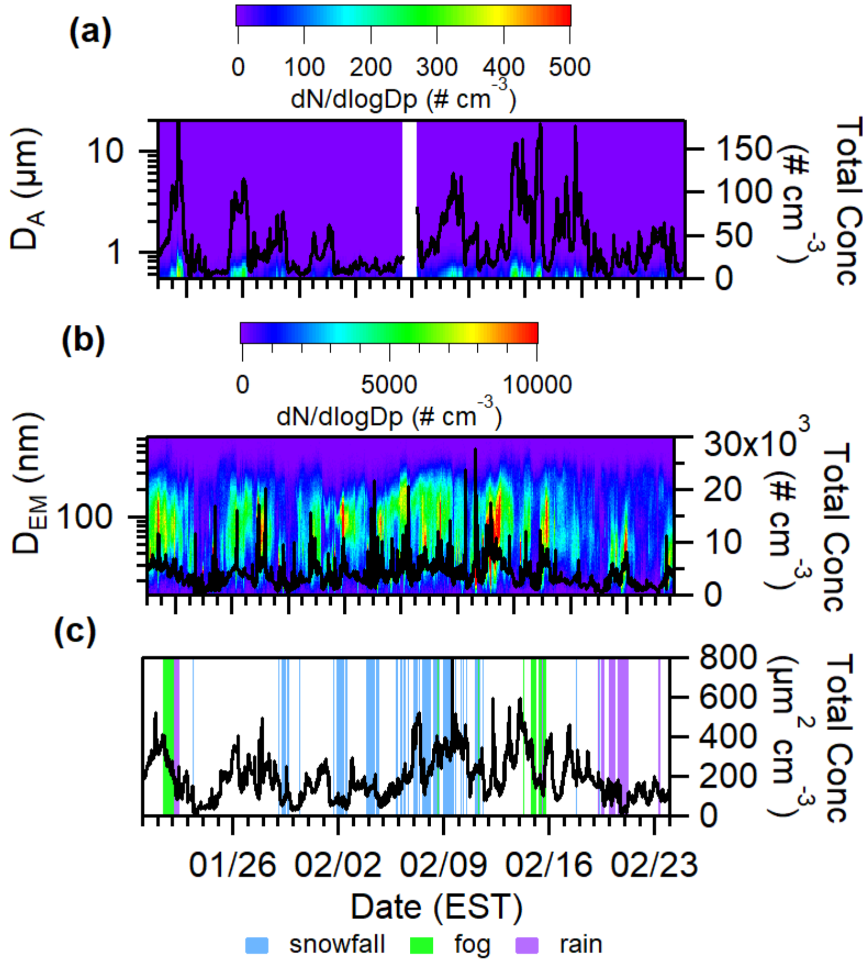

Figure S11: Temporal variations in (a) aerosol size distributions and total number concentrations from the aerodynamic particle sizer (APS, model 3321, TSI, Inc.), which measured aerodynamic diameter (D_A) from 0.5-20 µm, (b) aerosol size distributions and total number concentrations from the scanning mobility particle sizer (SMPS, model 3082, TSI, Inc.), which measured electrical mobility diameter (D_{EM}) from 14.1-736.5 nm, and (c) total (D_{EM} 14.1-736.5 nm) surface area concentrations measured by the SMPS, where shading represents the occurrence of snowfall (light blue), fog (green), and rainfall (purple).

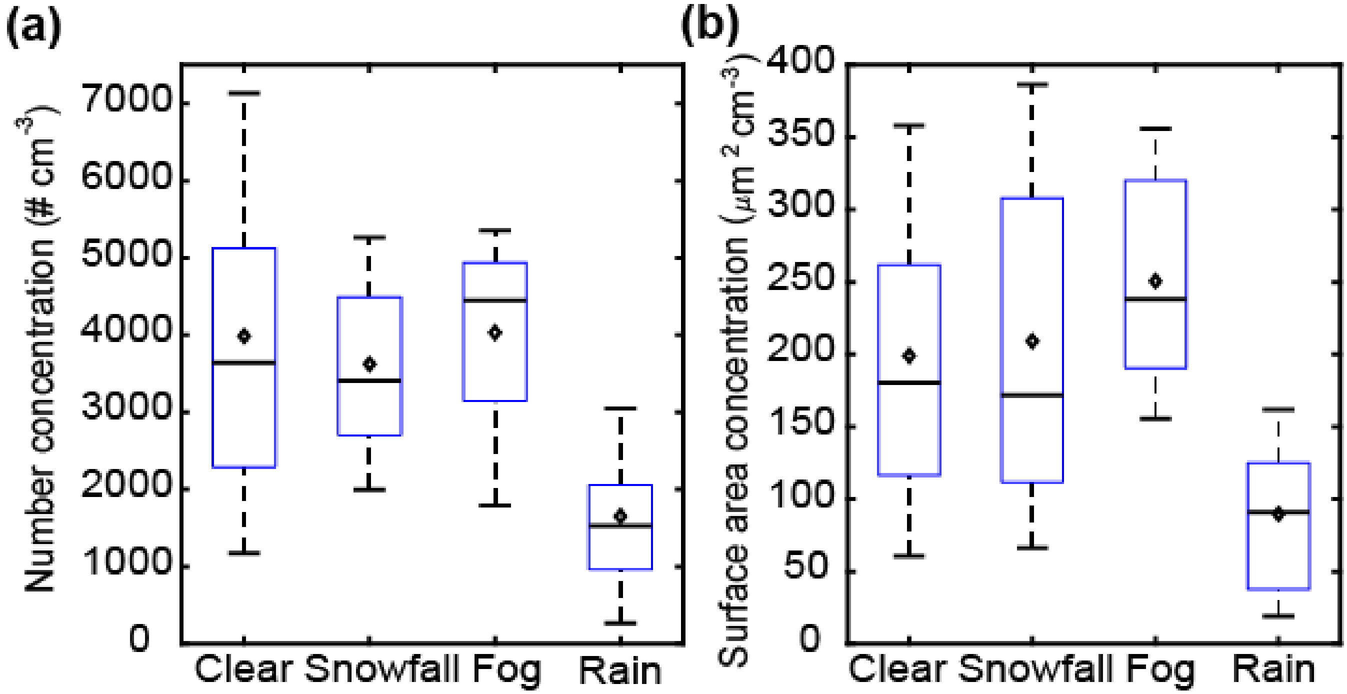

Figure S12: Box plots showing 30 min averaged submicron (D_{EM} 14.1-736.5 nm)) (a) number and (b) surface area concentrations during nighttime (18:00 – 08:00 EST) clear conditions and weather events (snowfall, fog, and rain) from January 20-February 24. Bars represent the 10th, 50th, and 90th percentiles, boxes represent the 25th and 75th percentiles, and diamonds represent the means. Number concentrations are not statistically significantly different between clear and snowfall conditions (p=0.06), clear and fog conditions (p=0.88), or between snowfall and fog conditions (p=0.06). Surface area concentrations are not statistically significantly different between clear and snowfall conditions (p=0.32). The remaining comparisons between aerosol concentrations across the weather conditions are statistically significant ($p<0.05$). Number concentrations were 2300±120 particles cm^{-3} (2.4 times) lower during rainfall in comparison to clear conditions. Surface area concentrations were 109±6 μm^{2} cm^{-3} (2.2 times) lower during rainfall, and 52±7 μm^{2} cm^{-3} (1.3 times) higher during fog, in comparison to clear conditions.

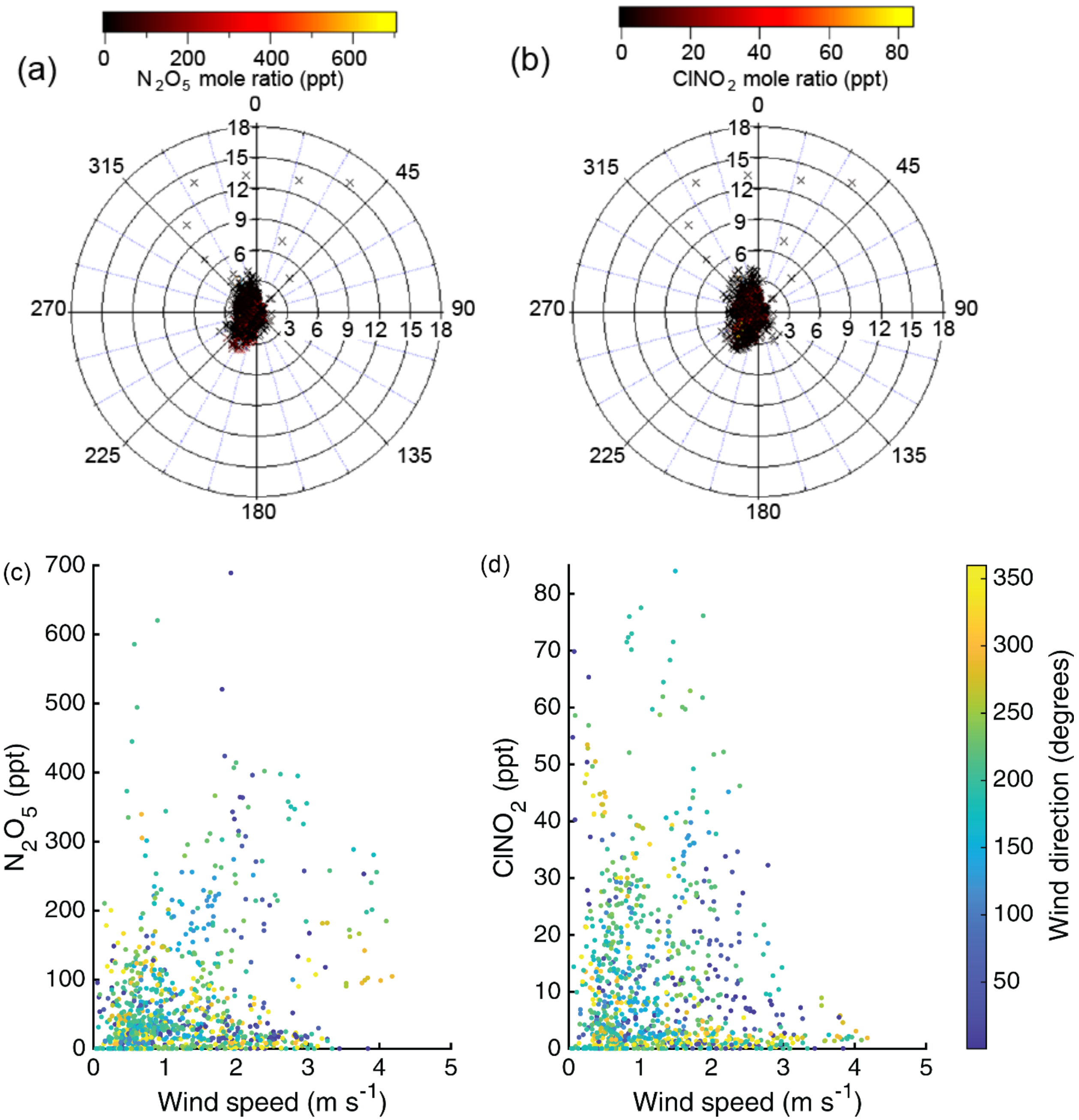

Figure S13: Polar plots show 30 min averaged wind direction (angle, degrees), 30 min averaged wind speed (radius, m s^{-1}), and 30 min averaged N_2O_5 mole ratios (a) and $ClNO_2$ mole ratios (b) on a colorscale. Plots of nighttime N_2O_5 mole ratios vs wind speed (c) and nighttime $ClNO_2$ mole ratios vs wind speed (d), with wind direction shown as a colorscale. No clear correlation is observed between wind speed or direction and N_2O_5 or $ClNO_2$ abundance.

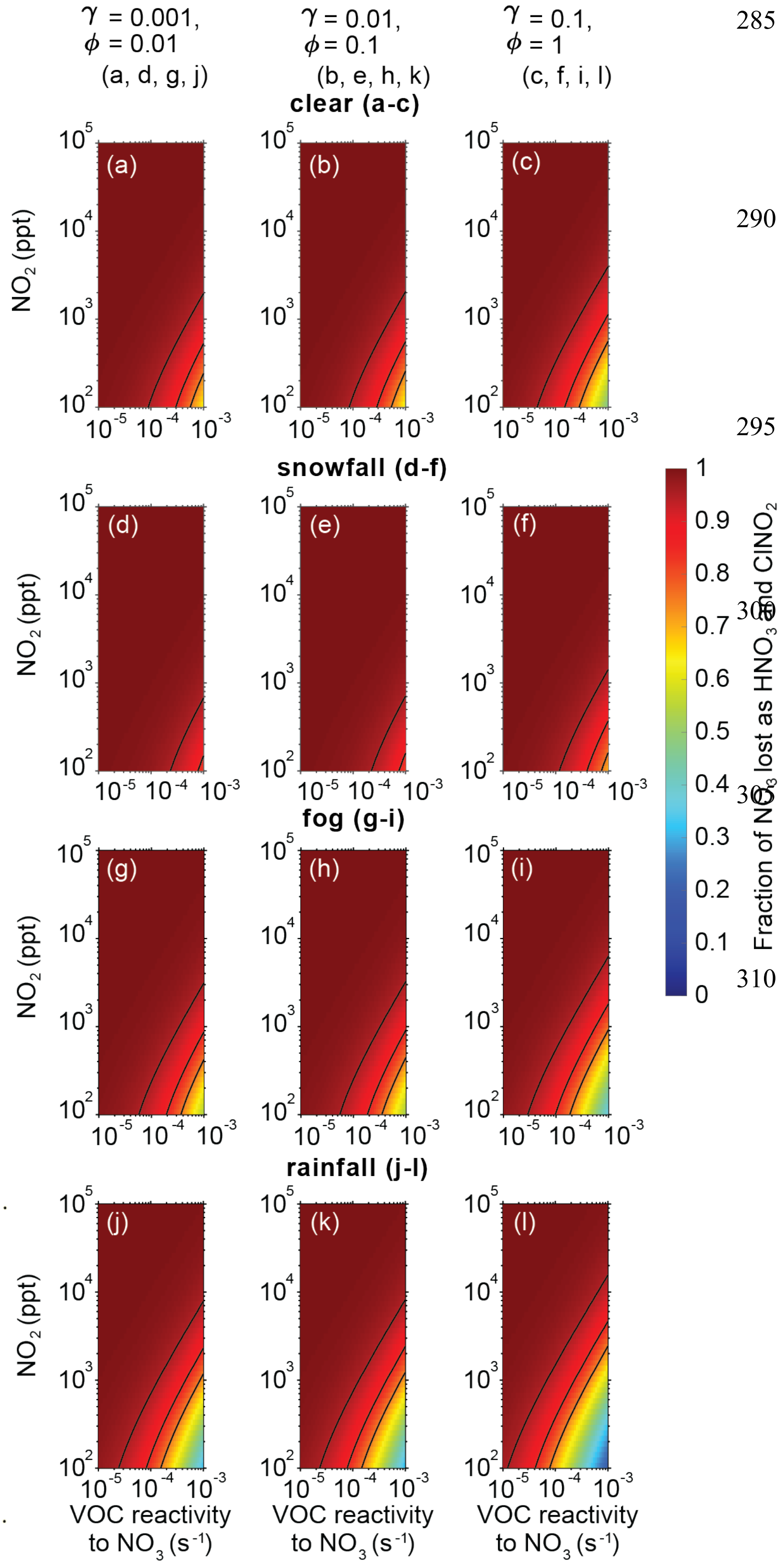

Figure S14: Fraction of NO_3 lost to inorganic pathways (i.e. through production of HNO_3 and $ClNO_2$, compared to reaction with VOCs), $\frac{P(\mathrm{HNO_3})+P(\mathrm{ClNO_2})}{P(\mathrm{HNO_3})+P(\mathrm{ClNO_2})+P(\mathrm{NO_3+VOC})}$, where $P(HNO_3)$ = HNO_3 production (R-S6), $P(ClNO_2)$ = $ClNO_2$ production (R-S7), and $P(NO_3+VOC)$ = reaction of NO_3 with VOCs (R-S4), plotted as a function of NO_2 mole ratio (ppt) and VOC reactivity to NO_3 (s^{-1}) for three different combinations of γ and φ (γ=0.001 and φ=0.01 [a, d, g, j], γ=0.01 and φ=0.1 [b, e, h, k], and γ=0.1 and φ=1 [c, f, i, l]). Black contour lines correspond to 75%, 85%, and 95% of NO_3 lost through inorganic pathways. When only two contours are shown, this corresponds to the 75th percentile off-scale, with only the 85th and 95th percentiles shown. Each set of three panels corresponds to each of the four case study nights: Jan 31-Feb 1 - clear (a-c), Feb 6-7 - snowfall (d-f), Feb 14-15 - fog (g-i), and Feb 20-21 - rainfall (j-l).

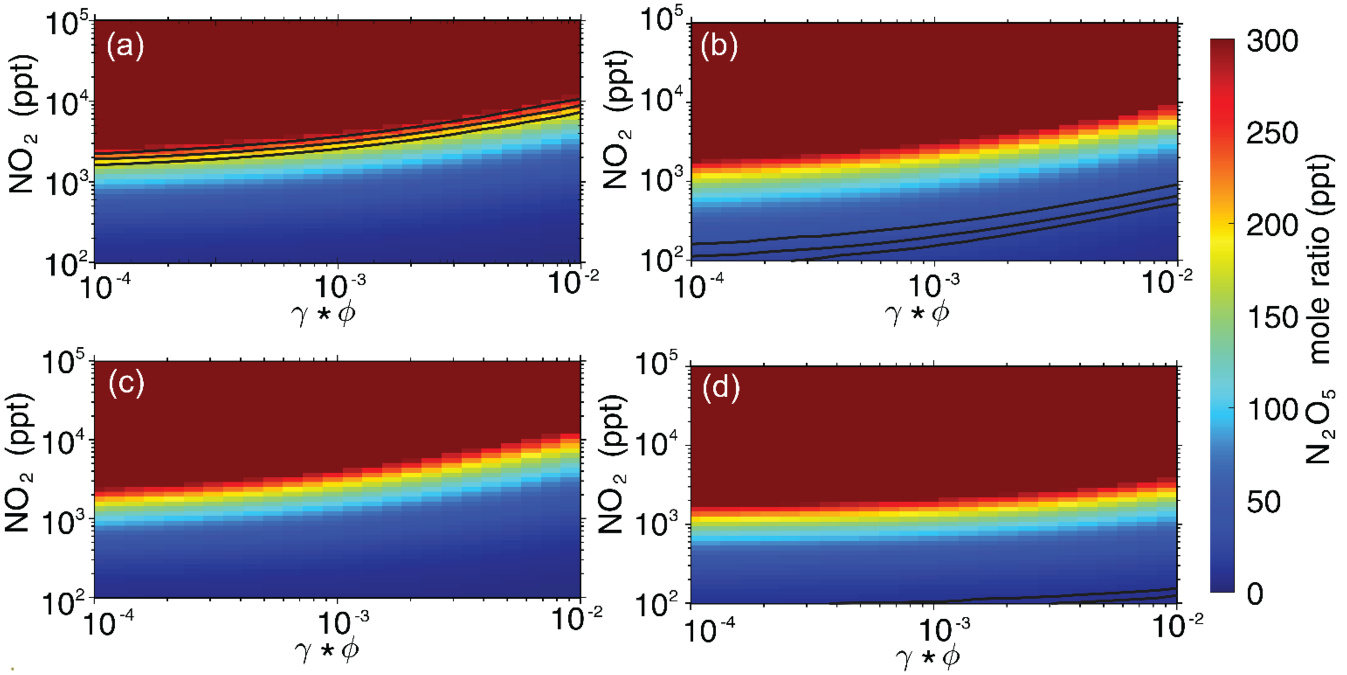

Figure S15: Simulated average N_2O_5 mole ratios from the final 4 h (corresponding to 04:00-08:00 EST) of a 14 h model run as a function of NO_2 mole ratio (ppt) and γ*φ products (N_2O_5 uptake * $ClNO_2$ yield) for the four case nights: Jan 31-Feb 1 - clear (a), Feb 6-7 - snowfall (b), Feb 14-15 - fog (c), and Feb 20-21 - rainfall (d). Contours represent the minimum, average, and maximum N_2O_5 mole ratios observed during the final 4 h of each case study period, with these values being offscale for the fog (c) and rainfall (d) cases, as discussed in Section S2. For these simulations, the reactivity of VOCs to NO_3 was held constant at 10^{-4} s^{-1}.

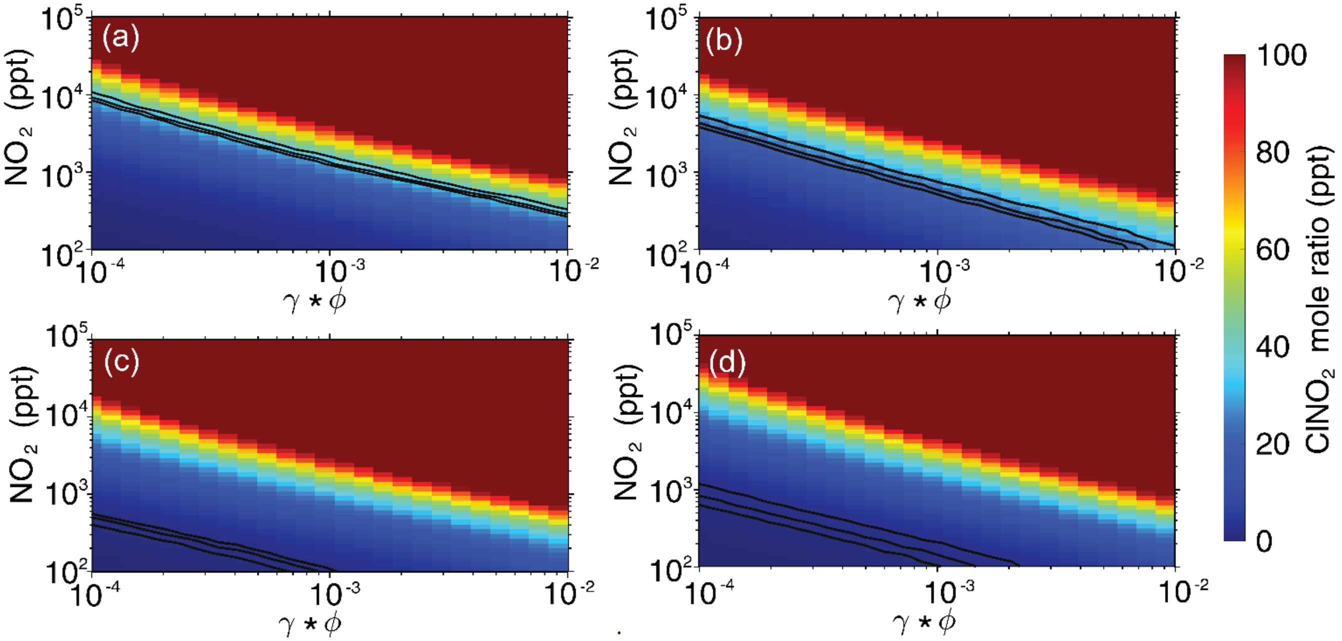

Figure S16: Simulated average $ClNO_2$ mole ratios from the final 4 h of a 14 h model run (meant to simulate the 18:00-08:00 nighttime period) as a function of NO_2 concentration (ppt) and $\gamma*\varphi$ products for the four case nights, Jan 31-Feb 1 - clear (a), Feb 6-7 - snowfall (b), Feb 14-15 - fog (c), and rainfall (d). Contours represent the minimum, average, and maximum $ClNO_2$ mole ratios observed during the final 4 h of each case study period. For these simulations, the reactivity of VOCs to NO_3 was held constant at 10^{-4} s^{-1}, as we determined previously (Fig S13) that the VOC loss pathway for NO_3 is minor in this wintertime MI environment.

Table S1: Ranges, medians, averages, and 95% confidence intervals for mole ratios of $ClNO_2$ and N_2O_5, $PM_{2.5}$ concentrations of Cl^- and NO_3^-, temperature, relative humidity (RH), and friction velocity (u*) measured across the entire campaign, between 18:00-08:00 EST. Data below the limit of detection (LOD) were applied as $\frac{1}{2}$×LOD in calculations.

	Clear	**Snowfall**	**Fog**	**Rain**
$ClNO_2$ range (ppt)	0.05-84	0.05-70	0.05-76	0.05-5.25
$ClNO_2$ median (ppt)	6.3	11.9	1.0	2.59
$ClNO_2$ average ± 95% confidence interval (ppt)	11.8±0.7	16.8±0.7	5.0±0.6	2.27±0.06
N_2O_5 range (ppt)	0.15-702	0.15-257	0.15-55	0.15-289
N_2O_5 median (ppt)	43	34	2.4	8
N_2O_5 average ± 95% confidence interval (ppt)	84±5	47±2	7.1±0.6	14±2
Cl^- range (μg m^{-3})	0.040-0.910	0.040-0.645	0.197-0.717	0.03-0.57
Cl^- median (μg m^{-3})	0.228	0.213	0.374	0.12
Cl^- average ± 95% confidence interval (μg m^{-3})	0.257±0.007	0.258±0.006	0.456±0.008	0.22±0.01
NO_3^- range (μg m^{-3})	0.03-3.9	0.07-2.50	0.11-3.9	0.027-0.707
NO_3^- median (μg m^{-3})	0.64	0.53	1.17	0.118
NO_3^- average ± 95% confidence interval (μg m^{-3})	0.95±0.04	0.81±0.03	1.38±0.04	0.126±0.007
Temperature range (K)	258.5-288.7	260.3-271.9	260.6-282.8	273.2-288.8
Temperature median (K)	271.2	264.9	277.3	283.3
Temperature average ± 95% confidence interval (K)	270.8±0.3	265.8±0.2	276.7±0.2	282.1±0.2
RH range (%)	39-97	64-97	73-100	39-97
RH median (%)	76.0	84.0	96.0	92.5
RH average ± 95% confidence interval (%)	75.0±0.5	82.9±0.3	93.7±0.3	90.2±0.4
u* range (m s^{-1})	0.032-0.498	0.027-0.509	0.029-0.719	0.03-0.74
u* median (m s^{-1})	0.133	0.102	0.123	0.30
u* average ± 95% confidence interval (m s^{-1})	0.150±0.004	0.129±0.004	0.162±0.007	0.36±0.01

Table S2: Ranges, medians, averages, and 95% confidence intervals for mole ratios of ClNO$_2$ and N$_2$O$_5$, PM$_{2.5}$ concentrations of Cl$^-$ and NO$_3^-$, temperature, relative humidity (RH), and friction velocity (u*) observed during each of the case study periods, between 18:00-08:00 EST. Data below the limit of detection (LOD) were applied as $\frac{1}{2}\times$LOD in calculations.

	Clear (Jan 31-Feb 01)	**Snowfall (Feb 06-07)**	**Fog (Feb 14-15)**	**Rain (Feb 20-21)**
ClNO$_2$ range (ppt)	1.5-45	2.4-70	0.6-4.5	0.6-3.7
ClNO$_2$ median (ppt)	21	28	1.6	1.8
ClNO$_2$ average ± 95% confidence interval (ppt)	23±5	30±6	1.8±0.4	2.0±0.3
N$_2$O$_5$ range (ppt)	75-274	22-201	1.1-31	7.1-40
N$_2$O$_5$ median (ppt)	207	71	2.7	11
N$_2$O$_5$ average ± 95% confidence interval (ppt)	200±16	82±21	5±3	13±4
Cl$^-$ range (μg m^{-3})	0.05-0.16	0.033-0.043*	0.037-0.065	0.023-0.028
Cl$^-$ median (μg m^{-3})	0.08	0.036*	0.042	0.026
Cl$^-$ average ± 95% confidence interval (μg m^{-3})	0.09±0.04	0.037±0.004*	0.047±0.04	0.026±0.03
NO$_3^-$ range (μg m^{-3})	0.7-1.7	0.3-1.2*	0.5-2.5	0.025-0.4
NO$_3^-$ median (μg m^{-3})	1.1	0.7*	0.7	0.1
NO$_3^-$ average ± 95% confidence interval (μg m^{-3})	1.2±0.4	0.7±0.3*	1.1±0.7	0.2±0.1
Temperature range (K)	273.1-276.6	263.7-266.1	276.0-282.8	273.2-287.6†
Temperature median (K)	274.6	265.0	280.1	278.2†
Temperature average ± 95% confidence interval (K)	274.8±0.4	265.1±0.3	279.7±0.9	279±2†
RH range (%)	62-76	63-88	92-100	85-93
RH median (%)	72	79	96	89
RH average ± 95% confidence interval (%)	72±1	78±3	96±1	89±1
u* range (m s^{-1})	0.07-0.23	0.02-0.13	0.11-0.28	2.2-8.9 (0.25-0.46) †
u* median (m s^{-1})	0.16	0.06	0.19	4.5 (0.46) †
u* average ± 95% confidence interval (m s^{-1})	0.16±0.01	0.06±0.01	0.18±0.02	5.0±0.5 (0.50±0.08) †

[*] Because the AIM-IC was not operational during the snowfall case study, the following night (February 07-08) is substituted for concentrations of Cl$^-$ and NO$_3^-$. The snowfall case study night and its substitution were similar in respect to snowfall and ground cover, but the substituted night had a higher friction velocity (average u*=0.12 m s^{-1}, whereas the snowfall case had an average u*=0.06 m s^{-1}).

[†] Because the sonic anemometer was not operational during the rainfall case, we use temperature and wind speed values from the Kalamazoo−Battle Creek International Airport (KAZO) located ~7 km to the southeast and retrieved from Weather Underground (https://www.wunderground.com/history/daily/us/mi/kalamazoo/KAZO). We provide estimated u* values in parentheses, calculated using the linear regression of u* vs wind speed in Figure S5.

Table S3: Mean aerosol surface area (14.1-736.5 nm), pressure, ozone mole ratios, and temperature for each case study night. These were were used as inputs for box modeling.

	Clear (Jan 31-Feb 01)	**Snowfall (Feb 06-07)**	**Fog (Feb 14-15)**	**Rain (Feb 20-21)**
Aerosol surface area (μm^2 cm^{-3})	199.0	209.1	250.7	89.8
Pressure (hPa)	975.3	995.6	978.1	988.8
Ozone (nmol mol^{-1}, ppb)	12.8	24.4	14.4	18.3
Temperature (K)	274.8	265.1	279.7	279.0

References

Bertram, T. H. and Thornton, J. A.: Toward a general parameterization of N_2O_5 reactivity on aqueous particles: the competing effects of particle liquid water, nitrate and chloride, Atmos. Chem. Phys., 9, 8351–8363, doi:10.5194/acp-9-8351-2009, 2009.

Kenagy, H. S., Sparks, T. L., Wooldridge, P. J., Weinheimer, A. J., Ryerson, T. B., Blake, D. R., Hornbrook, R. S., Apel, E. C. and Cohen, R. C.: Evidence of Nighttime Production of Organic Nitrates During SEAC4RS, FRAPPÉ, and KORUS-AQ, Geophys. Res. Lett., 47(11), 1–9, doi:10.1029/2020GL087860, 2020.

McDuffie, E. E., Fibiger, D. L., Dubé, W. P., Lopez Hilfiker, F., Lee, B. H., Jaeglé, L., Guo, H., Weber, R. J., Reeves, J. M., Weinheimer, A. J., Schroder, J. C., Campuzano-Jost, P., Jimenez, J. L., Dibb, J. E., Veres, P., Ebben, C., Sparks, T. L., Wooldridge, P. J., Cohen, R. C., Campos, T., Hall, S. R., Ullmann, K., Roberts, J. M., Thornton, J. A. and Brown, S. S.: $ClNO_2$ Yields From Aircraft Measurements During the 2015 WINTER Campaign and Critical Evaluation of the Current Parameterization, J. Geophys. Res. Atmos., 123(22), 12,994-13,015, doi:10.1029/2018JD029358, 2018.

McNamara, S. M., Kolesar, K. R., Wang, S., Kirpes, R. M., May, N. W., Gunsch, M. J., Cook, R. D., Fuentes, J. D., Hornbrook, R. S., Apel, E. C., China, S., Laskin, A. and Pratt, K. A.: Observation of Road Salt Aerosol Driving Inland Wintertime Atmospheric Chlorine Chemistry, ACS Cent. Sci., 5, doi:10.1021/acscentsci.9b00994, 2020.

McNamara, S. M., Chen, Q., Edebeli, J., Kulju, K. D., Mumpfield, J., Fuentes, J. D., Bertman, S. B. and Pratt, K. A.: Observation of N2O5 deposition and ClNO2 production on the saline snowpack, ACS Earth Sp. Chem., doi:10.1021/acsearthspacechem.0c00317, 2021.

Royer, H. M., Mitroo, D., Hayes, S. M., Haas, S. M., Pratt, K. A., Blackwelder, P. L., Gill, T. E. and Gaston, C. J.: The role of hydrates, competing chemical constituents, and surface composition on ClNO2formation, Environ. Sci. Technol., 55(5), 2869–2877, doi:10.1021/acs.est.0c06067, 2021.

Saunders, S. M., Jenkin, M. E., Derwent, R. G. and Pilling, M. J.: Protocol for the development of the Master Chemical Mechanism, MCM v3 (Part A): Tropospheric degradation of non-aromatic volatile organic compounds, Atmos. Chem. Phys., 3(1), 161–180, doi:10.5194/acp-3-161-2003, 2003.

Wang, S., McNamara, S. M., Kolesar, K. R., May, N. W., Fuentes, J. D., Cook, R. D., Gunsch, M. J., Mattson, C. N., Hornbrook, R. S., Apel, E. C. and Pratt, K. A.: Urban Snowpack ClNO2Production and Fate: A One-Dimensional Modeling Study, ACS Earth Sp. Chem., 4(7), 1140–1148, doi:10.1021/acsearthspacechem.0c00116, 2020.